

Study of Scintillator Strip with Wavelength Shifting Fiber and Silicon Photomultiplier.

V.Balagura^a M.Danilov^a B.Dolgoshein^b S.Klem in^b
 R.Mizuk^a P.Pakhlov^a E.Popova^b V.Rusinov^a
 E.Tarkovsky^a I.Tikhomirov^a

^aInstitute for Theoretical and Experimental Physics, B.Cheremushkinskaya 25,
 Moscow, 117259, Russia

^bMoscow Engineering and Physics Institute, Kashirskoe sh. 31, Moscow, 115409,
 Russia

Abstract

The performance of the 200 \times 2.5 \times 1 cm³ plastic scintillator strip with wavelength shifting fiber read-out by two novel photodetectors called Silicon Photomultipliers (SiPMs) is discussed. The advantages of SiPM relative to the traditional multichannel photomultiplier are shown. Light yield and light attenuation measurements are presented. This technique can be used in muon or calorimeter systems.

Key words: Scintillation detectors, wavelength shifting fibers, silicon photomultiplier

PACS: 29.40M, 29.40V

The detection of charged particles with plastic scintillators, wavelength shifting fibers and multichannel photomultipliers is a well known, efficient and robust technique (see, e.g. [1]). However it has severe limitations. First, photomultipliers can not work in the magnetic field. For scintillator counters inside a magnet one should bring the light out by clear fibers. This complexifies the detector and leads to some light losses. Second, fibers from different scintillator counters should be assembled together in a bundle attached to the multichannel photomultiplier. This is not always easy to arrange. Finally, calibration and monitoring of a multichannel photomultiplier is not a simple task.

In this work performed at ITEP (Moscow) we use the novel photodetector called Silicon Photomultiplier (SiPM) [2] instead of the traditional photomultiplier. It is the matrix of $1024 = 32 \times 32$ independent silicon photodiodes covering the area of $1 \times 1 \text{ mm}^2$. Each diode has its own quenching polysilicon resistor

of the order of a few hundred k. A diode-resistor pairs called pixels later on are connected in parallel. A common reverse bias V_{bias} is applied across them. Its magnitude of the order of 40{60 V is high enough to start the Geiger discharge if any free charge carrier appears in the p-n junction depletion region. The diode discharge current causes a voltage drop across the resistor. This reduces the voltage across the diode below the breakdown voltage $V_{breakdown}$ and the avalanche dies out. One diode signal is $Q_{pixel} = C_{pixel}(V_{bias} - V_{breakdown})$ where C_{pixel} is the pixel capacitance. Typically $C_{pixel} = 50 \text{ fF}$ and $V = V_{bias} - V_{breakdown} = 3V$ yielding $Q_{pixel} = 10^6$ electrons. Such an amplification is similar to the one of a typical photomultiplier and 3{4 orders of magnitude larger than the amplification of an Avalanche Photo Diode (APD) working in the proportional mode. Q_{pixel} does not depend on the number of primary carriers which start the Geiger discharge. Thus each diode detects the carriers created e.g. by a photon, a charged particle or by a thermal noise with the same response signal of 10^6 electrons. Moreover the characteristics of different diodes inside the SiPM are also very similar. When red, they produce approximately the same signals. This is illustrated in Fig. 1a. It shows the SiPM response spectrum when it is illuminated by weak flashes of a Light Emitting Diode (LED). The spectrum is obtained by integrating the SiPM signal during 120 nsec and using analog-to-digital converter. The integration time is big enough to contain most of the SiPM signal which lasts a few tenths of nsec. First peak in this figure is the pedestal. The second one is the SiPM response when it detects exactly one photon. It is not known which diode inside the SiPM produces the signal since all of them are connected to the same output. However since the responses of all pixels are similar, the peak width is small. If several pixels in the SiPM are red, the net charge signal is the sum of all charges. The third, forth and so on peaks in Fig. 1a correspond to 2, 3, ... red pixels. Note that the peaks are equidistant. If n pixels are red the corresponding peak width is approximately

$$n = \frac{q}{n^2 + \frac{2}{pedestal}}; \quad (1)$$

where $pedestal$ is the pedestal width and q describes the spread of signals Q_{pixel}^i from different pixels. For large n the peaks start to overlap and the spectrum loses its peak-like structure. This is illustrated in Fig. 1b which shows the SiPM response to the photons created by the minimum ionizing particle in the scintillator detector which will be discussed in detail in the rest of the paper. In this case the average number of red pixels is 8.4. This is still much smaller than the total number of pixels in the SiPM. Therefore the signal is approximately proportional to the number of photons and to the dE/dx losses in the scintillator. For even larger n the saturation effects come into play, and the whole dynamic range is limited by the finite number of SiPM pixels (1024

in our case ¹).

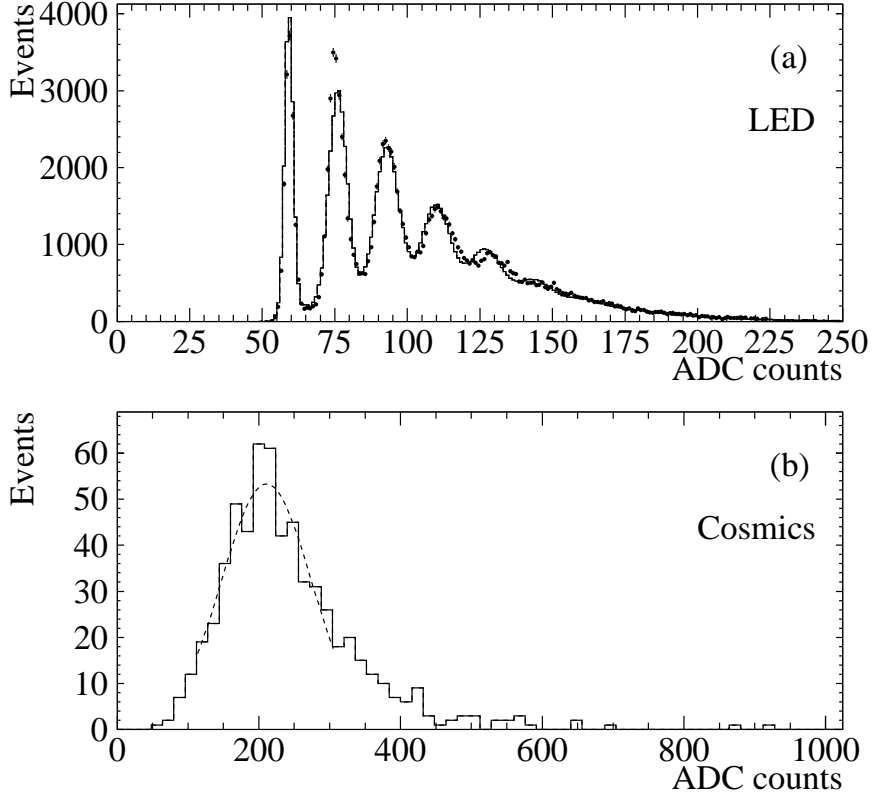


Fig. 1. SiPM signal spectra. (a): SiPM is illuminated by the short weak LED flashes. The fit curve is described in detail in Appendix A. (b): Typical SiPM response to cosmic particles. The dashed line shows the fit of the region around the peak to the Gaussian distribution.

The SiPM photodetection efficiency depends on the light wavelength and the overvoltage V . Typical value is about 10{15% for the green light. It includes geometrical inefficiency due to dead regions in the SiPM between the pixels. Thus SiPM and traditional photomultipliers have similar gain and efficiency. However, SiPM is approximately twice cheaper than one channel in the multichannel photomultiplier. In addition it can work in the magnetic field, so there is no need in the light transportation out of the magnetic field with clear fibers. SiPM is so tiny that it can be mounted directly on the detector. This minimizes the light losses because of a shorter fiber length. SiPM has a quite high noise rate of about 2 MHz at 0.1 photoelectron threshold. However the noise rate drops fast with increasing threshold. This will be discussed in more detail later.

¹ SiPMs can be produced with different number of pixels in the range 500{4000.

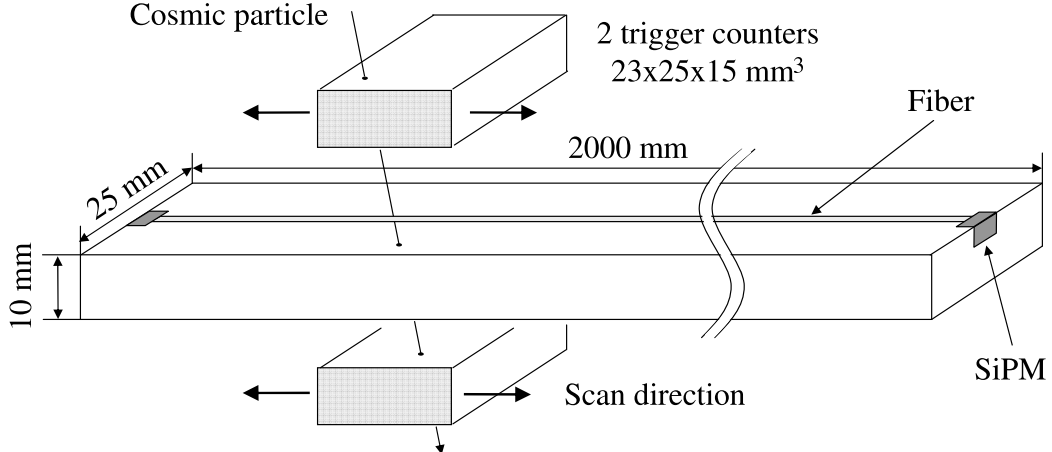


Fig. 2. The layout of the test bench (not in scale).

Our detector consists of a $200 \times 25 \times 1 \text{ cm}^3$ plastic scintillator strip and a wavelength shifting fiber read-out by two SiPMs installed at the strip ends (see Fig. 2). The scintillator strip is produced at the "Uniplast" enterprise in Vladimir, Russia. This is one of the biggest plastic scintillator producers in the world. The scintillator for the electromagnetic calorimeters of PHENIX, HERA-B and LHC-B experiments has been produced there. The strip is extruded from the granulated polystyrene with two dyes (1.5% of PTP and 0.01% POPOP). The Kuraray multicladning WLS fiber Y11 (200) with 1 mm diameter is put in the 2.5 mm deep groove in the middle of the strip. To improve the light collection efficiency, the strip is wrapped in the Superradiant VN2000 foil produced by the 3M company. No gluing is used to attach the WLS fiber to the SiPM or to the strip. There is about 200 μm air gap between the fiber end and the SiPM. It is a minimal gap which ensures that the fiber can not scratch the sensitive SiPM surface.

We use the cosmic particle trigger consisted of a pair of $2.3 \times 2.5 \times 1.5 \text{ cm}^3$ scintillator counters placed above and below the strip (see Fig. 2). The SiPM spectra like the one shown in Fig. 1b, are obtained for different positions of the trigger counters along the strip. The charge integration time is 120 nsec. In parallel to collecting the cosmic ray data, the strip is illuminated periodically by the short weak flashes of LED. The corresponding SiPM response spectrum shown in Fig. 1a has been already discussed. The distance between the peaks in Fig. 1a allows to calibrate the SiPM gain. Knowing the distance one can convert the ADC counts to the number of red SiPM pixels. This procedure is much easier than the calibration of a traditional photomultiplier.

To estimate the light yield of the detector for the minimum ionizing particle, we use the maximum of the Landau distribution (see Fig. 1b). The average value is approximately 1.1 times larger than the position of the maximum because of the Landau tail. We do not correct for this difference in order to be conservative in our estimates of the detector performance. To determine

the position of the maximum, the region around the Landau peak is fit to the Gaussian distribution as shown in Fig. 1b. The central value of the Gaussian is then transformed into the average number of red SiPM pixels using the calibration procedure described above.

Due to finite sizes of the trigger counters the selected cosmic particles are not strictly vertical. Thus they produce slightly more scintillation light than the minimum ionizing particle at normal incidence to the strip. To correct for this effect, a simple simulation is made. It assumes that the angular distribution of all cosmic particles coincides with the one of cosmic muons and has the form

$\cos^2 \theta$ where θ is the angle with respect to the vertical direction [3]. In this way it is found that in average the path length of triggered particles inside the scintillator is 10% larger than the strip thickness. Assuming that the light yield is also 10% larger, the measured average numbers of red SiPM pixels are divided by 1.1.

To convert them to the number of detected photons, another effect should be taken into account. There is an interpixel "cross-talk" inside the SiPM. The Geiger discharge of one diode can fire with some probability another diode and so on. The probability of firing of n extra diodes drops approximately exponentially with n . The effect increases with the applied voltage. In our case the average number of pixels fired by one initial photoelectron is found to be 1.43 for the left SiPM and 1.28 for the right one. It is determined from the fit of the spectrum in Fig. 1a. Without the interpixel cross-talk the peaks in Fig. 1a should correspond to the detection of 0, 1, 2 etc. photons. In this case the number of entries in the peaks should follow the Poisson law. The deviation from this law allows one to measure the cross-talk. The details of the procedure are described in Appendix A.

The measured numbers of red pixels in the left and right SiPM are divided by the cross-talk factors 1.43 and 1.28 respectively. The resulting average number of detected photons is plotted in Fig. 3 for different positions of the trigger counters along the strip. Filled triangles and open squares denote the left and right SiPM respectively. One can see that for the 2 m strip detector the transportation of light from the far end attenuates it by about a factor of 2. The upper filled circles in Fig. 3 show the sum of the two SiPM signals. It is uniform within 13%. Clearly, if position of the particle along the strip is known the uniformity can be significantly improved by applying the correction on the light attenuation. In the worst case when the particle passes through the strip center there are 13.7 detected photons. In case of Poisson statistics this corresponds to 98% efficiency at the threshold 7 photons. Such a high threshold is needed to reduce the SiPM noise rate. To express the same requirement in terms of red pixels a simple modelling is made. Instead of the sum of two SiPM signals we simulated the response of one SiPM to 13.7 Poisson distributed photons. The cross-talk and a SiPM single pixel peak width

from equation (1) are taken as the average of the corresponding values of two SiPMs. They are determined from the calibration spectra like in Fig. 1a. Since the two SiPMs have different gains, η is normalized to the distance between adjacent peaks before averaging. Further details on the simulation of the SiPM spectrum can be found in Appendix A. The left part of the modelled spectrum shows that 98% efficiency corresponds to the requirement to have 8 red pixels. With this requirement the efficiency averaged over the whole strip exceeds 99%.

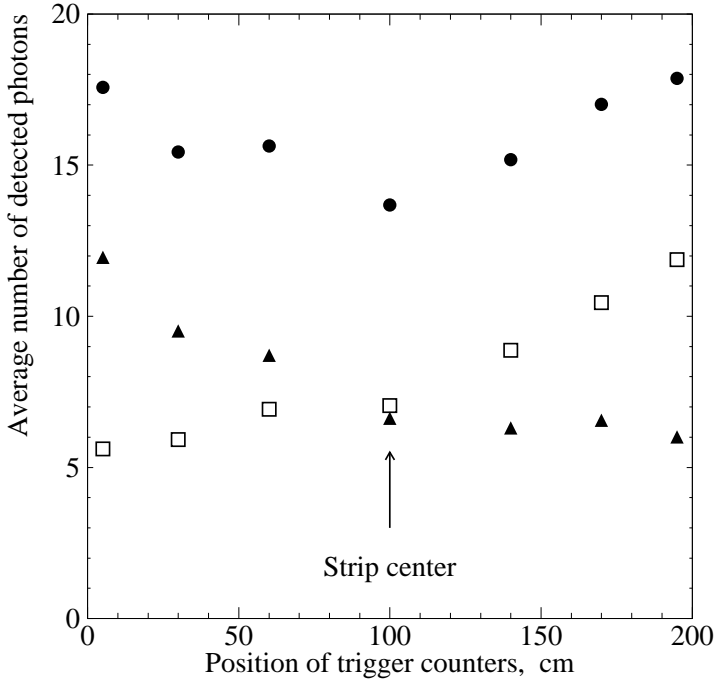


Fig. 3. Average number of photons detected by the left (triangles) and right (squares) SiPMs for normally incident cosmic ray particle versus the position of the trigger counters along the strip. The upper curve (filled circles) is the sum of the two SiPM signals.

This estimate can be checked with the data. It is convenient to express the SiPM response signals in terms of red pixels. This is achieved simply by shifting and scaling the ADC counts. Position of zero and the scaling factor are determined from the calibration spectrum like in Fig. 1a. The distribution of the number of pixels red in the two SiPMs by a cosmic particle is shown in Fig. 4. The top and bottom spectra correspond to two extreme cases when the particle passes through the center or the end of the strip. A few events around zero belong to the pedestal. It appears here due to imperfection of the trigger. The plots are not corrected for the factor 1.1 which was introduced above to take into account not normal incidence of cosmic particles. Therefore to estimate the efficiency of the requirement to have 8 red pixels for normal incidence one should count the entries between the pedestal and the

value 8 1:1 9. This part of the spectrum is hatched. There are 11 such events in the top plot. They correspond to the 1:7 0:5% inefficiency which agrees with the calculations above. The inefficiency averaged over all positions of the trigger counters along the strip is found to be 0:7 0:2%.

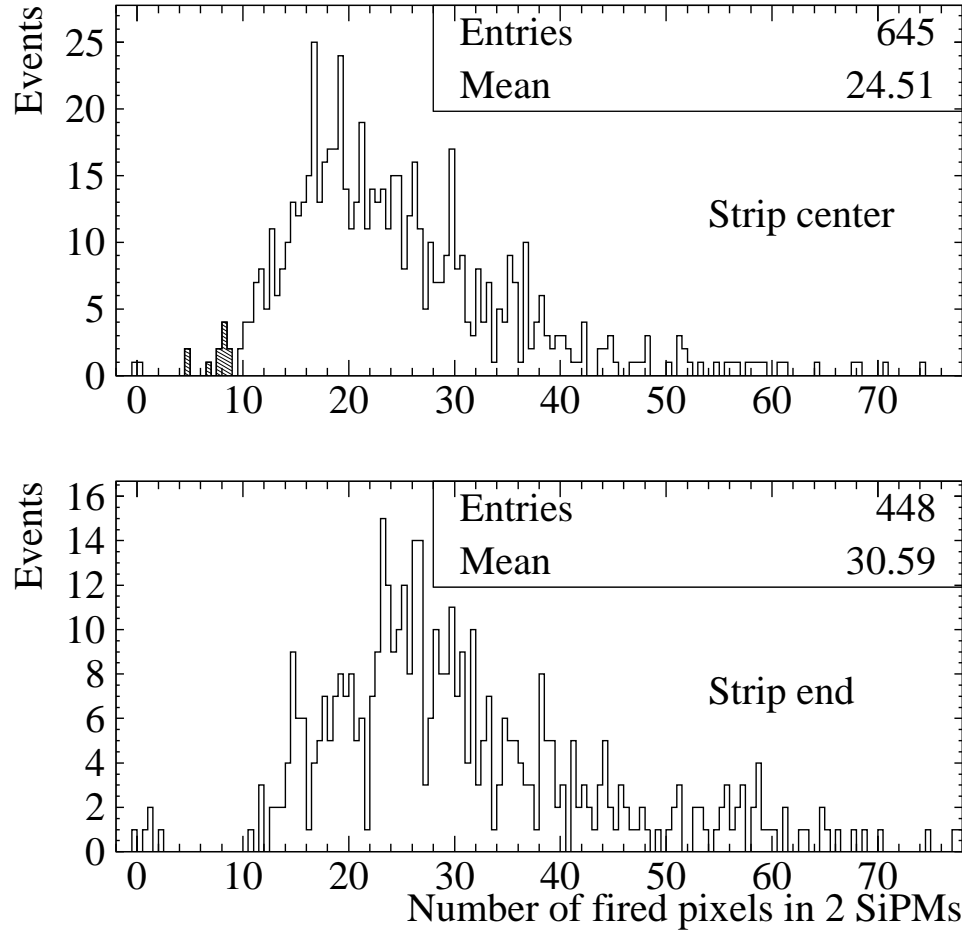


Fig. 4. Number of fired pixels in two SiPMs when trigger counters are located at the strip center (upper plot) and at the ends (lower plot).

The typical SiPM noise rate at a room temperature is shown in Fig. 5. It is measured without any trigger by counting the number of SiPM signals higher than a given threshold. The rate starts at about 2 MHz. The threshold value is again expressed in the units corresponding to one pixel signals. Therefore one can see clear steps at 1, 2, 3, 4 in the beginning of the plot. They correspond to the peaks in Fig. 1a. For larger signals the step-like structure becomes smeared and the rate drops approximately exponentially with the threshold. Since the SiPM signal is very short (~ 20 nsec) the probability that two independent noise signals overlap in time is small. Therefore big noise signals can be produced only by simultaneous correlated ring of several pixels caused

by the interpixel cross-talk. The exponential slope in Fig. 5 is thus determined by the cross-talk probability.

The rate of noise signals from two SiPMs with the threshold of 8 red pixels can not be directly read off the plot in Fig. 5. It depends on the type of the electronics which detects the coincidence between the SiPMs and calculates the total signal. As an example one can assume that the threshold is set for the sum of two SiPM signals integrated during the same 120 nsec gate which is used in obtaining the amplitude spectra in Fig. 4. Comparing the gate with the 2 MHz SiPM noise rate one can see that there is a sizeable probability that two or even more noise signals can contribute to the net signal. This changes the exponential slope in Fig. 5. The probability to get 8 red pixels in the random 120 nsec window is found to be 7×10^{-4} . It is measured with the random trigger. Clearly, the noise can be suppressed even further if the electronics utilizes the fact that two SiPM signals caused by real particles are closer in time than 120 nsec.

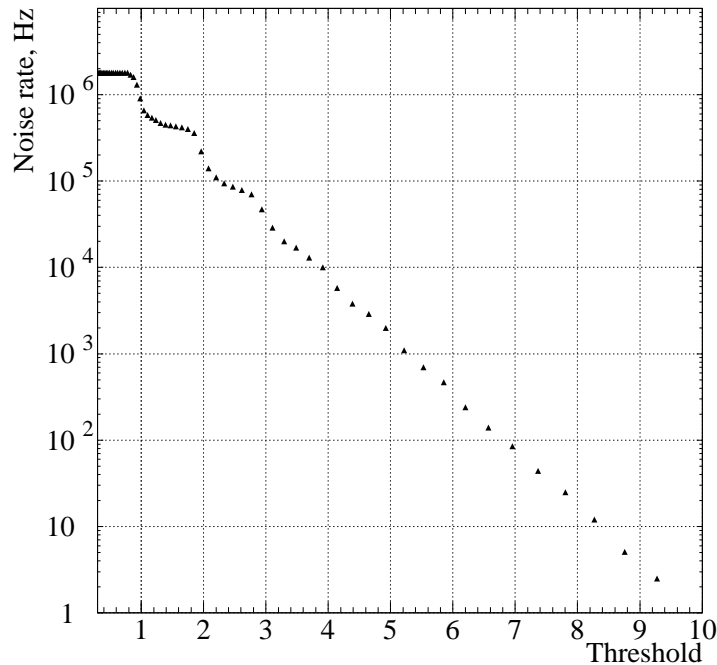


Fig. 5. Typical SiPM noise rate versus the threshold expressed in the units corresponding to one pixel signals.

In conclusion, the detector consisting of the 200 \times 2.5 \times 1 cm³ plastic scintillator strip, the wavelength shifter and two novel photodetectors called Silicon Photomultipliers has been constructed and tested. This new technique can be used in the muon systems or in calorimeters. For example it can be used in the muon system of the future International Linear Collider detector. The tested scintillator detector has higher efficiency and by far higher

rate capabilities than resistive plate chambers which are often used in muon systems. SiPM has similar gain and efficiency as the traditional multichannel photomultiplier. It also has several advantages. There is no need to use clear fibers to bring the light out of the magnetic field and to arrange many fibers in one bundle attached to the multichannel photomultiplier. SiPM can be mounted directly on the strip end. Its gain can be determined easily by observing the peaks corresponding to different number of red SiPM pixels (see Fig. 1a). Finally it is approximately twice cheaper than one channel in a multichannel photomultiplier. Further cost reductions are expected in case of a mass production. The light yield and light attenuation measurements for the tested scintillator strip detector are shown in Fig. 3. The light yield of more than 13 detected photons per cosmic ray particle at normal incidence is obtained. The light collection efficiency can be further increased by gluing the WLS fiber to the strip [4]. We plan to study this possibility systematically in the future.

A The fit procedure of the SiPM calibration spectrum

To calibrate the SiPM, it is illuminated by the LED flashes. A typical SiPM response spectrum is shown in Fig. 1a. This histogram is fit to the convolution of the pedestal spectrum (B) obtained with the random trigger when the LED is off and the SiPM response function (L) to the photons from LED which will be described later. Thus its Fourier transform which will be denoted in the following by L^F superscript can be written as $B^F L^F$. Assuming the stability of LED and the pure Poisson distribution of photons detected by SiPM, L^F can be written as

$$L^F = \sum_{n=0}^{\infty} \frac{e^{-P^F}}{n!} (P^F)^n = \exp(-P^F) (1 - g);$$

where P^F is the Fourier transform of the response to exactly one photon, g is the average number of photons detected by the SiPM. We use the fact that the response to n photons is n convolutions of P and thus has a Fourier transform $(P^F)^n$. Due to the interpixel cross-talk one photon can be more than one pixel. To describe this effect we approximate P^F by

$$P^F = \frac{G^F + (G^F)^2 + (G^F)^3 + \dots + (G^F)^k + \dots}{1 + +^2 + \dots + ^{k-1} + \dots} = G^F \frac{1}{1 - G^F};$$

where α describes the cross-talk probability, G^F is the Fourier transform of the SiPM signal distribution when exactly one random pixel in it is red. The average number of pixels red by one photon is $1 = (1 - \alpha)$. As an approximation

of G the Gaussian distribution is taken. Its sigma (σ), mean (μ) and also the cross-talk (α) are the only fit parameters. σ is equal to the distance between adjacent peaks in Fig. 1a. The number of photons N is constrained in the fit by the condition that the average of the histogram in Fig. 1a should be equal to the average of the background histogram B plus the average of L which is $\langle L \rangle = (1 - \alpha)$. Here we assume that the averages of experimental histograms when LED is on and off are known accurately and do not fluctuate.

If G and B functions are normalized so that they have unit integrals, the resulting formula for the Fourier transform of the α function is

$$N = B \exp \left(\frac{G^F - 1}{1 - G^F} \alpha \right);$$

where N is the total number of entries in the histogram. It is found that such a fit with 3 parameters can describe large variety of LED spectra for different SiPMs, bias voltages and LED intensities.

References

- [1] P. Adamson et.al, The MINOS scintillator calorimeter system, IEEE Trans. Nucl. Sci. 49 (2002) 861-863.
A. Pla-Dalmau, Extruded plastic scintillator for the MINOS calorimeters, in: 'Annecy 2000, Calorimetry in high energy physics', proceedings of 9th Conference on Calorimetry in High Energy Physics (CALOR 2000, Annecy, France), 513-522, preprint FERMILAB-CONF-00-343, (2001) 1-11.
D. F. Anderson et.al, Development of a low-cost extruded scintillator with co-extruded reflector for the MINOS experiment, preprint FERMILAB-CONF-00-261-E, (2000) 1-5.
- [2] G. Bondarenko et.al, Limited Geiger-mode silicon photomultiplier with very high gain, Nucl. Phys. Proc. Suppl. 61B (1998) 347-352.
G. Bondarenko et.al, Limited Geiger-mode microcell silicon photodiode: new results, Nucl. Instr. Meth. A 442 (2000) 187-192.
P. Buzhan et.al, An advanced study of silicon photomultiplier, ICFA Intstr. Bull. 23 (2001) 28-41.
P. Buzhan et.al, Silicon photomultiplier and its possible applications, Nucl. Instr. Meth. A 504 (2003) 48-52.
V. Andreev et.al, A high granularity scintillator hadronic calorimeter with SiPM readout for a Linear Collider detector, Nucl. Instr. Meth. A 540 (2005) 368-380, preprint DESY-04-143, LC-DET-2004-027 (2004) 1-17.
- [3] S. Eidelman et.al, Particle Data Group, Phys. Lett. B 592 (2004) 1.
- [4] MINOS collaboration for example reported a factor of 1.8 improvement in the light yield after gluing the fiber to the 1-4:1-800 cm³ strip with co-

extruded TiO₂ reactive coating, The MINOS Detectors, Technical Design Report, NuM IL-337 (1998), p 5-16.